# An analysis of the accuracy of magnetic resonance flip angle measurement methods



2010 Phys. Med. Biol. 55 6157

(http://iopscience.iop.org/0031-9155/55/20/008)

IOP PUBLISHING PHYSICS IN MEDICINE AND BIOLOGY

Phys. Med. Biol. **55** (2010) 6157–6174 doi:10.1088/0031-9155/55/20/008

# An analysis of the accuracy of magnetic resonance flip angle measurement methods

**Glen R Morrell**[1] **and Matthias C Schabel**

Utah Center for Advanced Imaging Research, Radiology Department, University of Utah, Salt Lake City, UT, USA

E-mail: glen.morrell@hsc.utah.edu

Received 3 May 2010, in final form 20 August 2010
Published 29 September 2010
Online at stacks.iop.org/PMB/55/6157

**Abstract**

Several methods of flip angle mapping for magnetic resonance imaging have been proposed. We evaluated the accuracy of five methods of flip angle measurement in the presence of measurement noise. Our analysis was performed in a closed form by propagation of probability density functions (PDFs). The flip angle mapping methods compared were (1) the phase-sensitive method, (2) the dual-angle method using gradient recalled echoes (GRE), (3) an extended version of the GRE dual-angle method incorporating phase information, (4) the AFI method and (5) an extended version of the AFI method incorporating phase information. Our analysis took into account differences in required imaging time for these methods in the comparison of noise efficiency. PDFs of the flip angle estimate for each method for each value of true flip angle were calculated. These PDFs completely characterize the performance of each method. Mean bias and standard deviation were computed from these PDFs to more simply quantify the relative accuracy of each method over its range of measurable flip angles. We demonstrate that the phase-sensitive method provides the lowest mean bias and standard deviation of flip angle estimate of the five methods evaluated over a wide range of flip angles.

(Some figures in this article are in colour only in the electronic version)

## Introduction

The excitation flip angle in MRI varies across the imaging volume because of inhomogeneity of the transmit radio-frequency (RF) field ($B_1$). Precise measurement of flip angle allows correction of spatial variations in image intensity (Axel *et al* 1987, McVeigh *et al* 1986, Moyher *et al* 1995, Roemer *et al* 1990), has important applications in $T_1$ mapping and

[1] Author to whom any correspondence should be addressed.

  

quantitation of absolute contrast concentration in dynamic contrast-enhanced MRI (Deoni *et al* 2003, Schabel and Morrell 2009, Schabel and Parker 2008) and is necessary for parallel transmission (Katscher *et al* 2003, Zhu 2004), where individual RF coil field maps are needed for RF waveform calculation.

Several methods of flip angle mapping have been proposed, which differ in their sensitivity to noise in the image data on which flip angle estimates are based. The accuracy of each method varies with the actual flip angle. The most complete characterization of the performance of a flip angle mapping method is the probability density function (PDF) of the flip angle estimate it produces for a given true flip angle and given system SNR. We have evaluated the performance of flip angle mapping methods by deriving the PDF of the flip angle estimate produced by each method for each of a range of values of true flip angle, for a few different values of system SNR. From these PDFs we have also calculated the mean bias and standard deviation of the flip angle estimates, as a simpler but less complete way of portraying their accuracy.

We evaluate the accuracy of five methods of flip angle measurement:

(1) The phase-sensitive method, which uses the phase difference between two acquisitions as a measure of actual flip angle (Morrell 2008).
(2) The gradient recalled echo (GRE) dual-angle method in which two acquisitions are performed with different nominal flip angles (Cunningham *et al* 2006, Insko and Bolinger 1993, Kerr *et al* 2007, Stollberger and Wach 1996).
(3) A modified dual-angle GRE method which takes the phase of the acquisitions into account (Insko and Bolinger 1993), which we refer to as the 'extended dual-angle method.'
(4) The 'actual flip angle imaging' (AFI) method (Yarnykh 2007), which utilizes two acquisitions interleaved in a GRE sequence with equal flip angle but different TR.
(5) A modified AFI method which takes the phase of the acquisitions into account, which we refer to as the 'extended AFI method.'

Each of these methods is evaluated by calculating the PDF of the flip angle estimate obtained by the method for a range of values of the actual flip angle, based on corruption of the source MR image with Gaussian white noise. The mean bias and standard deviation of error for the five methods are compared.

One previous study has been performed (Wade and Rutt 2007) comparing B1 mapping methods with Monte Carlo simulation. That study showed an advantage to the phase-sensitive method, but details of implementation of the phase-sensitive method were different than that proposed in Morrell (2008), which appeared in print later. No analysis by propagation of PDFs was performed in Wade and Rutt (2007). We have previously presented a subset of the current work (Morrell and Schabel 2009). This paper develops the concepts suggested in Morrell and Schabel (2009) and adds comparison to the extended GRE and extended AFI methods.

## Theory

Each of the five methods of flip angle mapping uses an excitation scheme that encodes information about the actual flip angle in image data. In the case of the dual-angle GRE methods and the AFI methods, the information about the actual flip angle is encoded in the ratio of the magnitudes of two image acquisitions. In the case of the phase-sensitive method, the flip angle information is encoded in the phase of the image acquisitions. The corruption of acquired image data by measurement noise limits the accuracy with which flip angle may be determined. We evaluate the impact of this noise on the various methods by calculating the PDF of the flip angle estimate obtained by each method for each of a range of actual flip angles. Our starting point is the assumption that image data are corrupted with Gaussian white

noise, with variance determined by the system SNR, as defined in appendix A.1. From this we derive the PDF of the magnitude of each acquisition for the dual-angle and AFI methods or the phase of each acquisition for the phase-sensitive method. The derivation of magnitude and phase PDFs is given in appendix A.2. The PDF is then propagated through the function used by each method to estimate the flip angle from the measured quantity. The result is the PDF of the flip angle estimate.

*Phase-sensitive $B_1$ mapping method*

The phase-sensitive method of flip angle measurement (Morrell (2008)) forms an image after a $2\alpha$ flip about the $x$-axis followed immediately by an $\alpha$ flip about the $y$-axis, and the phase of this image is measured. A second image is formed from an acquisition with the $2\alpha$ initial excitation reversed in sign. The phase of this image is also measured. The difference in phase between the two is a monotonic function of the flip angle $\alpha$ from which $\alpha$ can be calculated. Details of the derivation of the PDF of the flip angle estimate for the phase-sensitive method are given in appendix A.3.

*Dual-angle method with GRE*

In the dual-angle method with GRE, two images are formed. The first image is acquired after excitation with a flip angle $\alpha$ and has magnitude proportional to $\sin(\alpha)$. The second image is acquired after excitation with a flip angle $2\alpha$ and has magnitude proportional to $\sin(2\alpha)$. The ratio of the two acquisitions is formed giving

$$r = \frac{\sin\alpha}{\sin 2\alpha} = \frac{1}{2\cos\alpha}, \tag{1}$$

from which the flip angle $\alpha$ can be calculated. The details of the derivation of the PDF of the flip angle estimate for the dual-angle GRE method are given in appendix A.4.

*Extended dual-angle GRE method*

In the dual-angle GRE method, flip angles from 180° to 90° give magnitude ratios equal to those obtained for flip angles between 0° and 90°, symmetric about 90°. For instance, the signal magnitude ratio for $\alpha = 70°$, $2\alpha = 140°$ is the same as that for $\alpha = 110°$, $2\alpha = 220°$. For this reason, the dual-angle GRE method is only valid over a range of flip angles $\alpha$ from 0° to 90°. However, the dual-angle GRE method can be extended to a range of flip angles $\alpha$ from 0° to 180° by examining the phase of the two acquisitions. For flip angles $\alpha$ from 0° to 90°, the two acquisitions have the same phase, while for flip angles from 90° to 180° the phase of the two acquisitions differs by 180°. Thus by examining the relative phase of the two acquisitions, a range of flip angles from 0° to 180° can be mapped. We have designated this approach the 'extended dual-angle GRE' method. The derivation of the PDF of the flip angle estimate for the extended dual-angle GRE method is detailed in appendix A.5.

*AFI method*

In this method two images are formed during a single sequence in which spoiled GRE acquisition is performed from alternating $\alpha$ excitations following two different repetition times $TR_1$ and $TR_2$, with $TR_2 > TR_1$. The ratio $r$ of the magnitudes of the two images is formed and the flip angle $\alpha$ is estimated as

$$\alpha \approx \cos^{-1}\left(\frac{rn-1}{n-r}\right), \tag{2}$$

where $n = TR_2/TR_1$. Appendix A.6 contains the details of the derivation of the PDF of the flip angle estimate for the AFI method.

*Extended AFI method*

The AFI method gives flip angle estimates in a range of 0° to about 104°. The exact value of the maximum measurable flip angle depends on $T_1$ and on the choice of $TR_1$ and $TR_2$. Above this range, the method gives erroneous estimates in a manner similar to the dual-angle GRE method, in this case being roughly symmetric about the maximum angle of about 104° rather than 90°. Flip angles from about 105° to 180° will give estimates ranging roughly from about 104° to 0°. However, similar to the dual-angle GRE method, the AFI method gives signal acquisitions which are in phase for flip angles from 0° to about 104°, and opposite in phase for flip angles from about 104° to 180°. If this phase is taken into account, a range of 0° to 180° can be measured. The derivation of the PDF of the flip angle estimate for the extended AFI method is given in appendix A.7.

*SNR efficiency*

The dual-angle and phase-sensitive methods of $B_1$ mapping require a somewhat long TR to allow signal regeneration after presaturation. In the case of the phase-sensitive method, this presaturation is required because the excitation used in the phase-sensitive $B_1$ mapping method leaves some residual longitudinal magnetization $M_z$ which varies as a function of true flip angle $\alpha$. Variation of $M_z$ is not usually a problem since the flip angle estimate depends on the phase of the transverse magnetization, not its amplitude. However, for some flip angles the residual $M_z$ may be negative, which could alter the sign of the phase of the subsequent excitation. For this reason, a presaturation pulse is used to reset $M_z$ to zero at the end of each acquisition. The dual-angle GRE method is also implemented with a presaturation pulse (Cunningham *et al* 2006) or very long TR to eliminate $T_1$ dependence of the flip angle estimate. In contrast, the AFI method can operate with short TR. Therefore, comparison of these methods requires that their TR requirements be taken into account. This is done by simulating multiple signal averages for the AFI techniques, or equivalently, decreasing the standard deviation of the image noise for the AFI techniques compared to the phase-sensitive and dual-angle methods. This is discussed in more detail below for the specific choice of parameters used in our analysis.

## Methods

For each of the five methods of flip angle measurement, the PDF of the flip angle estimate was calculated for a range of actual flip angles. The PDFs were calculated according to the equations given in appendixes A.3 through A.7 with custom scripts in MATLAB (Mathworks, Natick, MA). The mean bias and standard deviation of the flip angle estimates were also calculated for comparison.

*Choice of parameters for comparison*

The accuracy of the dual-angle methods and the phase-sensitive method depends in part on the choice of TR and the $T_1$ of the sample, as these will affect the longitudinal magnetization $M_z^-$ available for each excitation. Assuming a sequence repetition time TR and a minimum amount

of time $TR_{min}$ required to complete the excitation, readout and presaturation pulse, a time TR–$TR_{min}$ is available before each excitation for regeneration of the longitudinal magnetization $M_z$. Given an equilibrium longitudinal magnetization $M_0$, the longitudinal magnetization $M_z^-$ available at the beginning of excitation is

$$M_z^- = M_0(1 - e^{-(TR-TR_{min})/T_1}). \tag{3}$$

Thus, the magnitude of the image depends on the $T_1$ of the sample being imaged. The image magnitude will affect the variance of the flip angle estimate. For the AFI method, TR and $T_1$ have more complex effects on the flip angle estimate, with increasing systemic error in estimation for shorter $T_1$. For purposes of direct comparison of flip angle mapping methods, concrete choices of sequence parameters and sample properties must be made. We have chosen to implement the AFI method with $TR_1 = 30$ ms and $TR_2 = 150$ ms, as suggested in Yarnykh (2007). This gives a total sequence TR of 180 ms. The dual-angle techniques and the phase-sensitive technique have TR requirements similar to each other, as both incorporate presaturation to reset $M_z$ prior to each excitation. We have chosen a TR of 540 ms for both of these methods, which is in line with implementations described in Cunningham *et al* (2006) and Morrell (2008). A minimum repetition time $TR_{min}$ is required for excitation, readout (typically echo-planar or spiral) and presaturation. We have set $TR_{min}$ to 40 ms, giving a regeneration interval of TR–$TR_{min} = 500$ ms for presaturation recovery. Since the dual-angle and phase-sensitive techniques require two complete acquisitions, each of which takes three times the duration of the AFI technique (180 ms * 3 = 540 ms), the signal acquired in the AFI method is averaged six times, giving a decrease in the standard deviation of the measurement noise for the AFI method by a factor of $\sqrt{6}$. The performance of the phase-sensitive method varies somewhat with off-resonance frequency. For this analysis, we assume no off-resonance.

### *Out-of-bounds measurements*

Each of the flip angle estimation methods measures a quantity on which flip angle estimates are based. For the phase-sensitive method, this quantity is the difference in phase between two images. For the dual-angle and AFI methods, this quantity is the ratio of the magnitude of two images. In all of the methods, the measured quantity has an allowed range. For instance, there is no flip angle for which the ratio of acquisitions in the AFI methods or dual-angle methods can theoretically exceed 1. Since the actual measurements are corrupted by noise, some measurements will fall into a range that is not theoretically possible and which does not generate a valid flip angle measurement. We denote these measurements as 'out of bounds.' We have dealt with out-of-bounds measurements in our analysis by discarding these measurements and renormalizing the PDF to have area 1 over the range of valid flip angles. Another approach would be to accept out-of-bounds measurements but assign them to the flip angle which would be most likely to give this measurement, i.e. a ratio greater than 1 would map to a flip angle estimate of 0° for the AFI method and 90° for the non-extended dual-angle method.

### *Range of the flip angle estimation method*

The dual-angle GRE technique is valid over a range of flip angles from 0° to 90°. The AFI technique is valid over flip angles from 0° to approximately 100°. The extended dual-angle, extended AFI and phase-sensitive methods are valid from 0° to 180°. To allow fair comparison, each method is evaluated over a range of 0 to $2\alpha_{nom}$, where $\alpha_{nom}$ represents the middle of the valid range for that method. For the double angle method $\alpha_{nom} = 45°$, for the AFI method

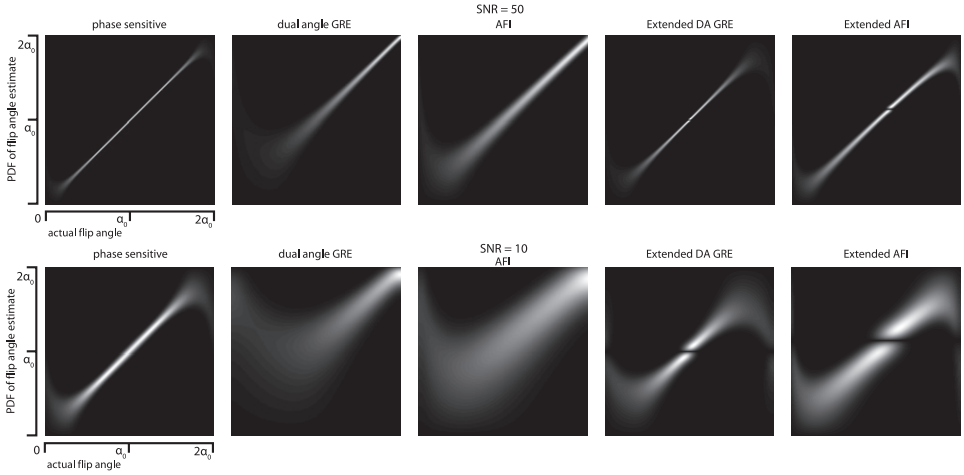


**Figure 1.** Probability density functions (PDFs) for flip angle estimates obtained by five flip angle measurement techniques over a range of actual flip angles for two values of the system SNR. Each image represents a set of PDFs for multiple actual flip angles for a given measurement method. A single vertical line from each image represents the PDF for the flip angle estimate at a particular actual flip angle. A perfect flip angle measurement technique would appear as a line along the diagonal. The top row shows the flip angle estimate PDFs for a system SNR of 50, while the bottom row shows the PDFs for a system SNR of 10. Difference in required imaging time for the AFI methods has been taken into account in these results, i.e. the PDFs shown for the AFI method and the extended AFI method represent flip angle estimates formed from the average of six signal acquisitions. Results are expressed in terms of a nominal flip angle $\alpha_0$ at the middle of the measurable range for each method. For the phase-sensitive method and the extended dual-angle and extended AFI methods, $\alpha_0 = 90^\circ$. For the standard (non-extended) dual-angle method, $\alpha_0 = 45^\circ$, and for the standard AFI method $\alpha_0 = 50^\circ$.

$\alpha_{\text{nom}} = 50^\circ$, and for the extended dual-angle, extended AFI and phase-sensitive methods $\alpha_{\text{nom}} = 90^\circ$.

### *Effect of $T_1$ on flip angle measurement accuracy*

To investigate the effect of variations in $T_1$ on the accuracy of the five methods, each method was simulated with $T_1$ values of 200 ms, 500 ms and 800 ms.

### *Accuracy criteria*

The PDF of the flip angle estimate a gives complete information on the accuracy of each method. Some insight into the specific features of the performance of each method is gained by examining the PDFs of the flip angle estimates for a range of actual flip angles, as in figure 1. For ease of depiction, the mean and standard deviation of the flip angle estimate are also calculated from the PDF. The likelihood of an out-of-bounds measurement for a given actual flip angle is also depicted.

### *Verification with Monte Carlo simulation*

The PDF formulas presented above were verified by Monte Carlo simulation of flip angle estimation with each method for two values of system SNR. Histograms of the flip angle estimate under Monte Carlo simulation were compared to plots of the equations and found to agree.

## Results

The performance of each method of flip angle measurement is most easily visualized by inspection of the PDF of the flip angle estimate for each of a range of actual flip angles. This is depicted in figure 1 for all five methods at two different values of system SNR for $T_1$ of 500 ms. In this figure, the PDFs are portrayed as an image, with each vertical column of image pixels representing the PDF of the flip angle estimate for a given actual flip angle so that a perfect flip angle estimation method would be represented by a line along the diagonal. Figure 1 shows that the phase-sensitive method most closely approaches this ideal, followed by the extended dual-angle method and the extended AFI method, with the non-extended dual-angle and AFI methods giving the worst results.

For ease of comparison, the mean bias and standard deviation of the flip angle estimates for all five methods at two different values of system SNR are plotted in figures 2 and 3. These plots show that both the mean bias and standard deviation of the flip angle estimate are lowest for the phase-sensitive method over most of the range of flip angles. The standard dual-angle and AFI methods both give large mean bias at low flip angles and become more accurate with increasing flip angle. The PDFs illustrated in figure 1 show that at low flip angles these two methods may give little useful information about the actual flip angle. In contrast, the phase-sensitive and extended dual-angle and AFI methods show performance which is relatively symmetric about $\alpha_0$. None of the methods performs well for flip angles near zero.

Figure 4 shows a plot of the probability of an 'out-of-bounds' measurement for each of the five methods over a range of actual flip angles. The probability of an out-of-bounds measurement becomes significant for all of the methods at very low flip angles, but is generally lower for the phase-sensitive method than the other methods over a wide range of flip angles. Out-of-bounds measurements are also possible at the upper limit of the range of flip angles for the phase-sensitive and extended dual-angle and AFI methods.

Figure 5 shows the effect of variation in $T_1$ on the accuracy of each method, with mean bias and standard deviation of the flip angle estimates plotted for $T_1$ values of 200 ms, 500 ms and 800 ms.

Figure 6 demonstrates a typical Monte Carlo simulation result for one flip angle measurement method at one SNR for one actual flip angle compared to the closed form equations. Similar comparison was made for the entire range of actual flip angles with all five methods at two different values of system SNR, verifying the correctness of the equations.

## Discussion

### *Accuracy of flip angle mapping methods*

The phase-sensitive method of flip angle measurement gives lower mean bias and lower standard deviation of flip angle estimates over a wide range of flip angles when compared with the other four methods considered here. After the phase-sensitive method, the extended dual-angle and extended AFI methods have the next best performance. Both the dual-angle and AFI methods are substantially improved by incorporating phase information from the two signal acquisitions. Extending these methods to include phase information increases the range of flip angles they can measure, and thus decreases the relative mean bias and standard deviation of their flip angle estimates. Inspection of the PDFs shown in figure 1 reveals that the extended dual-angle method never returns a flip angle estimate of 90°, and that the extended AFI method never returns an estimate of 104° (for the given choice of sequence parameters).

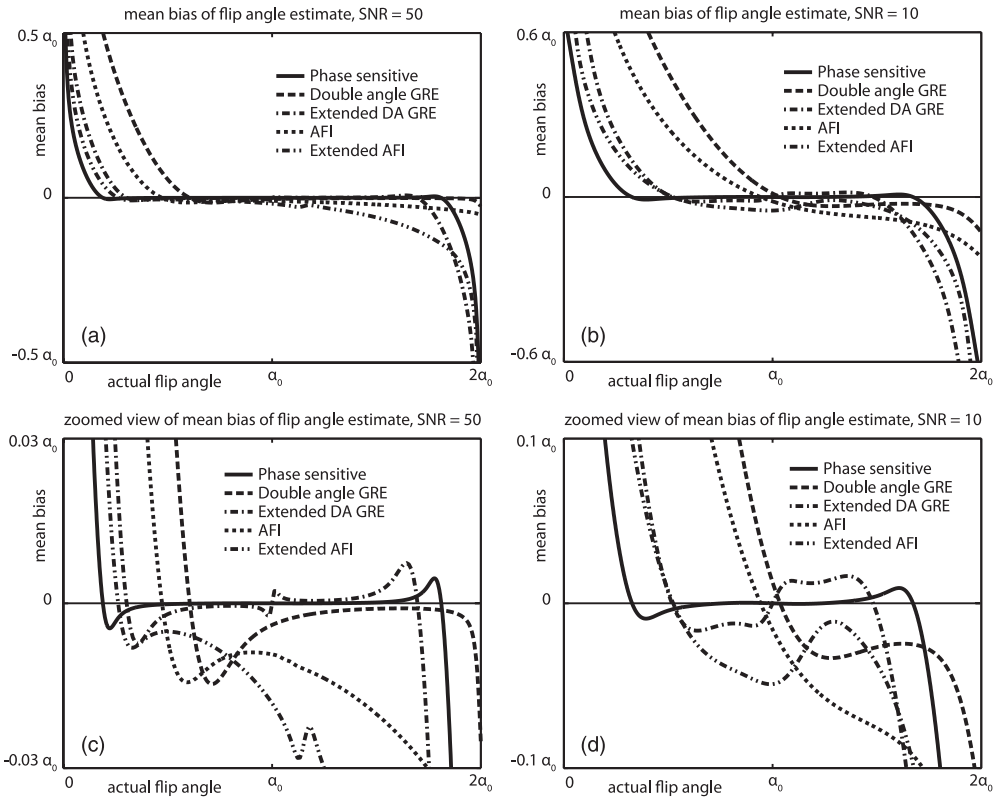


**Figure 2.** Mean bias of flip angle estimates for five methods of flip angle measurement. Panel A shows the mean bias for a system SNR of 50. Panel B shows mean bias for SNR of 10. Panel C is a zoomed-in view of panel A to show finer detail around zero. Panel D is a zoomed-in version of panel B. For the phase-sensitive, extended dual-angle and extended AFI methods, $\alpha_0 = 90^\circ$. For the dual-angle method, $\alpha_0 = 45^\circ$. For the AFI method, $\alpha_0 = 50^\circ$. Results for the AFI method and the extended AFI method reflect six signal averages.

This idiosyncracy is caused by singularities in the functions $g(\mathbf{r})$ which relate the measured magnitude ratios $\mathbf{r}$ to the flip angle estimates. This example shows how the PDFs of the flip angle estimate give a more complete picture of the performance of the various methods than simply comparing their mean bias and standard deviation of error.

We have expressed the mean bias and standard deviation of the flip angle estimate obtained by each method in terms of an angle $\alpha_0$ in the middle of the measurable range of the method rather than in units of degrees. These units seem to be most appropriate for actual flip angle mapping scenarios. For instance, when mapping the flip angle achieved by a transmitting surface coil, a method that can map flip angles from $0^\circ$ to $180^\circ$ with an accuracy of $\pm 2^\circ$ would be more useful than a method that can map angles from $0^\circ$ to $90^\circ$ with the same absolute accuracy of $\pm 2^\circ$. The accuracy of the method relative to its entire usable range is usually the important quantity since the assumption of a linear relationship between flip angle and RF amplitude is routinely made. Therefore, the mean bias and standard deviation of flip angle estimates are best expressed in terms of the entire dynamic range of the method used rather than in absolute units such as degrees. There may be situations in which the absolute

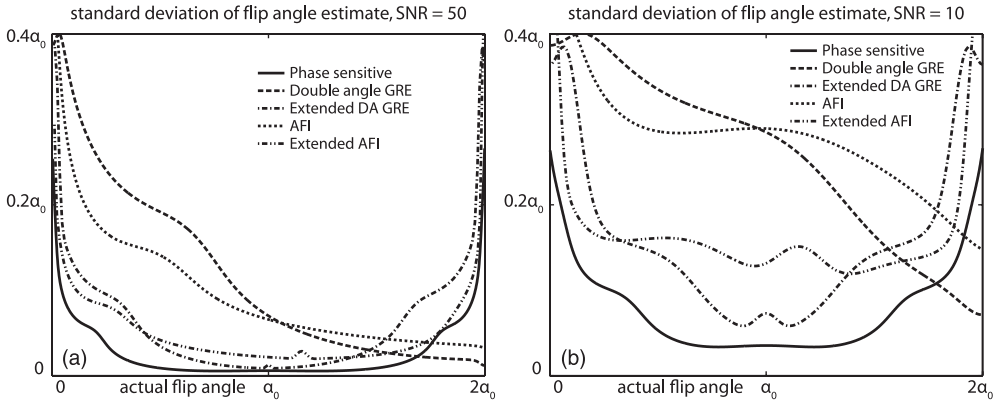


**Figure 3.** Standard deviation of the flip angle estimate for five methods of flip angle measurement. Panel A shows results for a system SNR of 50. Panel B shows results for a system SNR of 10. For the phase-sensitive, extended dual-angle and extended AFI methods, $\alpha_0 = 90^\circ$. For the dual-angle method, $\alpha_0 = 45^\circ$. For the AFI method, $\alpha_0 = 50^\circ$. Results for the AFI method and the extended AFI method reflect six signal averages.

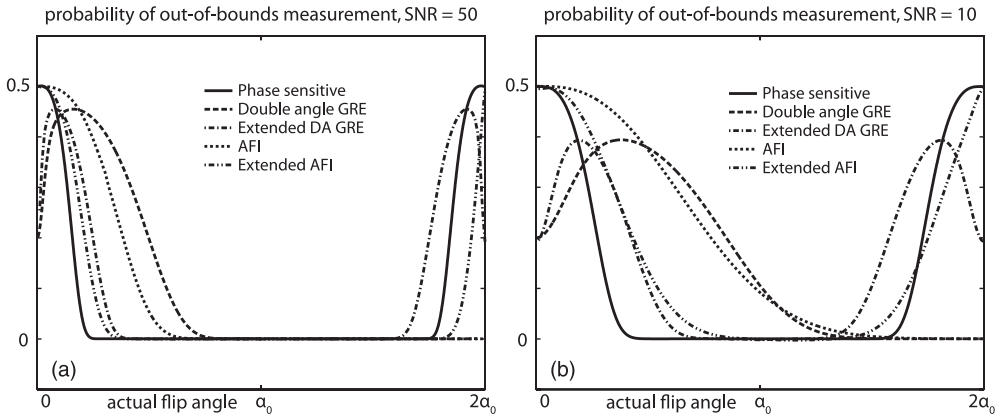


**Figure 4.** Probability of out-of-bounds measurement for various values of actual flip angle for the five flip angle measurement methods. Panel A shows probability of out-of-bounds measurement for SNR of 50. Panel B shows probability of out-of-bounds measurement for SNR of 10. For the phase-sensitive, extended dual-angle and extended AFI methods, $\alpha_0 = 90^\circ$. For the dual-angle method, $\alpha_0 = 45^\circ$. For the AFI method, $\alpha_0 = 50^\circ$. Results for the AFI method and the extended AFI method reflect averaging of six signal acquisitions before determining whether the measurement is out-of-bounds.

flip angle is important. In these situations, a method with larger dynamic range such as the phase-sensitive method may have additional advantages beyond relative accuracy.

### *Effect of $T_1$ on accuracy of flip angle estimates*

The flip angle methods investigated vary in their sensitivity to $T_1$. If used with short sequence repetition time, the dual-angle methods are sensitive to $T_1$ variations. For this reason, the dual-angle methods are typically used with long TR or with presaturation before each excitation, to make the $T_1$ weighting of the images obtained with $\alpha$ and $2\alpha$ flip angle excitations equal so that they cancel out when the ratio of the two acquisitions is formed (Cunningham *et al*

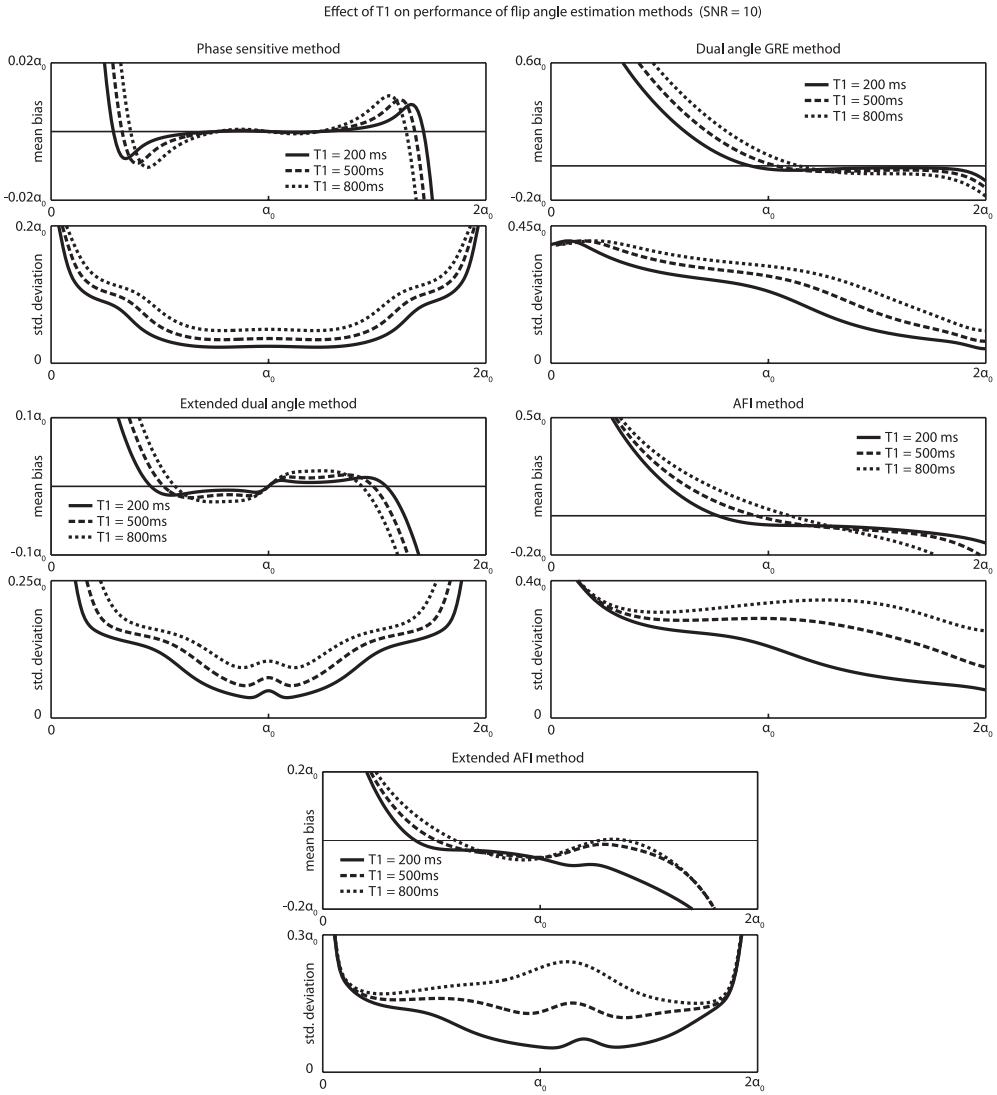


**Figure 5.** Effect of $T_1$ on the accuracy of flip angle estimates obtained by the five methods. Increasing $T_1$ has the same effect on the phase-sensitive and dual-angle methods as decreasing the system SNR. The effect of $T_1$ on the accuracy of the AFI methods is more complicated.

2006). Our analysis has assumed presaturation. With this assumption, varying $T_1$ affects the dual-angle methods only by varying the longitudinal magnetization $M_z^-$ available after the regeneration period before each excitation, as expressed in equation (3). Thus, varying the $T_1$ has the same effect on the accuracy of the dual-angle methods as varying the system SNR. For instance, an increase in $T_1$ from 500 ms to 800 ms with a regeneration interval of 500 ms results in a 26% decrease in the available signal, which is equivalent to a 26% decrease in the system SNR.

The phase-sensitive method is insensitive to $T_1$ variation, as the phase of the signal does not vary with $T_1$. For some flip angles, the longitudinal magnetization after the $2\alpha$-$\alpha$ excitation may be negative. This could invert the phase of the subsequent excitation. To avoid

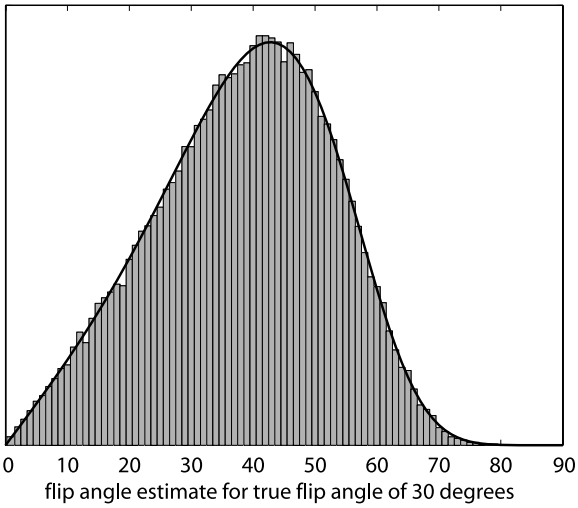


**Figure 6.** Typical Monte Carlo simulation result verifying correctness of the closed form equations used to calculate PDFs. This figure shows a histogram of flip angle estimates using the AFI technique with six signal averages for an actual flip angle of 30° and a system SNR of 10, with 100 000 iterations. The solid line is the PDF calculated by the closed-form equations. Similar agreement between Monte Carlo histograms and calculated PDFs was verified for all five methods at 1° increments of flip angle over the measurable range of flip angles with two different values of the system SNR.

this possibility, the phase-sensitive method has been implemented with presaturation (Morrell 2008). Our analysis has assumed presaturation. Thus, the effect of $T_1$ variation on flip angle estimates with the phase-sensitive method is the same as with the dual-angle methods, with longer $T_1$ decreasing the available magnetization $M_z^-$, having the same effect as the lower system SNR.

The AFI methods are affected by $T_1$ in a more complicated fashion than the other methods. Figure 5 shows the effect on mean bias and standard deviation of the flip angle estimate of varying $T_1$.

### *Effect of readout schemes on flip angle estimates*

In practice, the phase-sensitive method and the dual-angle methods have been implemented with presaturation and fairly long TR. This necessitates the use of fast readout schemes such as echo-planar acquisition to maintain reasonable imaging times (Morrell 2008, Cunningham *et al* 2006). In contrast, the AFI method has been implemented with rapid GRE acquisition (Yarnykh 2007). Our analysis has focused only on the intrinsic information present in the signal created by the excitation scheme for each method and does not depend on the particular readout scheme used for signal acquisition. Our results do take into account the difference in required TR between the methods, but are independent of the readout scheme used. For instance, if the phase-sensitive method were implemented with a simple GRE readout, with one line of k-space acquisition after each excitation, it would take about six times the imaging time of the AFI method with the same GRE acquisition. This difference in required imaging time is explicitly taken into account in the results presented above in that we averaged six signal acquisitions for the AFI method for every one acquisition of the other methods. (Equivalently, the standard deviation of the image noise was decreased by a factor of $\sqrt{6}$ for the AFI method).

The difference in required imaging time between the AFI method and the other methods would be about the same if all methods were implemented with a rapid echo-planar readout or some other readout scheme. Details of readout implementation have little effect on the accuracy of the methods.

*Other factors influencing the choice of flip angle methods*

Practical implementation issues may favor the use of one method over another. For instance, the phase-sensitive method has been implemented with rapid non-selective RF pulses which require 3D imaging over the entire sensitive volume of the receive coil, which may lead to long imaging times (Morrell 2008). This method is less suitable for single-slice flip angle mapping. The dual-angle and AFI techniques have been implemented as single-slice excitations for improved imaging speed, but this approach introduces errors in flip angle estimation due to averaging of flip angle over slice profiles (Cunningham *et al* 2006). The AFI method can be implemented in a rapid GRE configuration but has been shown to be very sensitive to RF and gradient spoiling issues (Nehrke 2009). Our analysis focuses only on the intrinsic accuracy possible with each technique, independent of other practical considerations.

## Conclusion

We have analyzed five methods of flip angle mapping by calculating the PDF of the flip angle estimate over a range of actual flip angles. We compared the phase-sensitive method, the dual-angle method with GRE acquisition, an extended dual-angle GRE method which takes the phase of the acquisitions into account, the AFI method and an extended AFI method including phase information. Our analysis shows that performance of the dual-angle and AFI methods is greatly improved by extending their range of measurable flip angles by incorporating phase information. This increased range results in smaller relative errors in $B_1$ estimation. However, the phase-sensitive method was found to give estimates of flip angle with lower mean bias and standard deviation than the other methods, including the extended versions of the dual-angle and AFI methods, over a wide range of actual flip angles for equivalent imaging times.

## Acknowledgment

Grant support: NCI 5K08CA112449-04, NIBIB K25EB005077-05.

## Appendix

*A.1. Definition of image noise and system signal to noise ratio (SNR)*

The complex value of a given voxel of an MR image at spatial location $(x, y, z)$ can be expressed as

$$\mathbf{S}(x, y, z) = \mathbf{A}(x, y, z) + \mathbf{n}(x, y, z), \tag{A.1}$$

where $\mathbf{A}(x, y, z)$ is the noise-free image and $\mathbf{n}(x, y, z)$ is the noise contribution. For the purpose of our analysis of the accuracy of flip angle mapping methods, we will assume a uniform signal level and a uniform noise standard deviation over the entire imaging volume and we will drop the explicit dependence on spatial location from subsequent notation. The noise sample $\mathbf{n}$ can be expressed as the sum of two noise components (Henkelman 1985):

$$\mathbf{n} = n_{\perp} + in_{\parallel}, \tag{A.2}$$

with $n_\perp$ and $n_\parallel$ independent Gaussian white noise samples with zero mean and the same standard deviation $\sigma$. The orientation of $n_\parallel$ can be defined as parallel to the signal vector $\mathbf{A}$, and $n_\perp$ as orthogonal to $\mathbf{A}$. We define SNR as

$$\mathrm{SNR} = \frac{|\mathbf{A}_0|}{\sigma}, \tag{A.3}$$

where $|\mathbf{A}_0|$ represents the maximum signal amplitude that can be achieved with a perfect 90° excitation and infinite TR with no signal loss from T1 or T2 effects.

### *A.2. Magnitude and phase noise*

The signal $\mathbf{A}$ can be expressed as a vector $\mathrm{A} = A_x\hat{x} + A_y\hat{y}$ in the $x$–$y$ imaging plane. The noise-corrupted signal in a given pixel can then be expressed as $\mathbf{S} = (A_x + n_x)\hat{x} + (A_y + n_y)\hat{y}$ where $n_x$ and $n_y$ are independent Gaussian white noise samples with standard deviation $\sigma$. We can define random variables $\mathbf{x}$ and $\mathbf{y}$ representing the $x$- and $y$-components of the noise-corrupted signal, and their joint PDF is

$$f_{\mathbf{x},\mathbf{y}}(x, y) = \frac{1}{2\pi\sigma^2}\exp\left(-\frac{(x - A_x)^2 + (y - A_y)^2}{2\sigma^2}\right), \tag{A.4}$$

i.e. the PDF of the noise-corrupted signal is a two-dimensional Gaussian distribution with mean $(A_x, A_y)$.

If we express the complex signal $\mathbf{A}$ in terms of magnitude $\rho$ and phase $\phi$ as $\mathbf{A} = \rho\,\mathrm{e}^{\mathrm{i}\phi}$, we can define the random variable $\mathbf{m} = |\mathbf{A} + \mathbf{n}|$ as the magnitude of the noise-corrupted signal, and the random variable $\mathbf{\Phi} = \arg(\mathbf{A} + \mathbf{n})$ as the phase of the noise-corrupted signal. Then, the joint PDF of $\mathbf{m}$ and $\mathbf{\Phi}$ can be found by converting equation (A.4) to polar coordinates:

$$f_{\mathbf{m},\mathbf{\Phi}}(m, \Phi) = \frac{m}{2\pi\sigma^2}\exp\left(-\frac{m^2 - 2m\rho(\cos\Phi\cos\phi + \sin\Phi\sin\phi) + \rho^2}{2\sigma^2}\right). \tag{A.5}$$

The PDF of the random variable $\mathbf{m}$ has the Rician density (Papoulis 1984):

$$f_{\mathbf{m}}(m) = \frac{m}{\sigma^2}I_0\left(\frac{m\rho}{\sigma^2}\right)\exp(-(m^2 + \rho^2)/2\sigma^2), \tag{A.6}$$

which is obtained by integrating equation (A.5) with respect to $\Phi$, with

$$I_0(x) = \frac{1}{2\pi}\int_0^{2\pi}\mathrm{e}^{x\cos\theta}\,\mathrm{d}\theta \tag{A.7}$$

the modified Bessel function. For $\sigma \ll \rho$, $\mathbf{m}$ has approximately a Gaussian distribution (Haykin 2001) with $\mathbf{m} \sim N(\rho, \sigma)$.

### *A.3. Phase noise*

The PDF of the phase $\mathbf{\Phi}$ is found by integrating equation (A.5) with respect to $m$, and is given by (Blachman (1981))

$$f_{\mathbf{\Phi}}(\Phi) = \frac{1}{2}\exp\left(-\frac{\rho^2}{2\sigma^2}\right) + \frac{\rho\cos(\Phi - \phi)}{2\sqrt{2\pi}\sigma} \times \exp\left(-\frac{\rho^2}{2\sigma^2}\sin^2(\Phi - \phi)\right)\mathrm{erfc}\left(-\frac{\rho}{\sqrt{2}\sigma}\cos(\Phi - \phi)\right), \tag{A.8}$$

where the complementary error function is defined as

$$\mathrm{erfc}(u) = \frac{2}{\sqrt{\pi}}\int_u^\infty \exp(-z^2)\,\mathrm{d}z. \tag{A.9}$$

For $\sigma \ll \rho$, the phase noise $\mathbf{\Phi} - \phi$ can be approximated as

$$\begin{aligned}\mathbf{\Phi} - \phi &\approx \tan^{-1}(n_\perp/\rho) \\ &\approx \sin^{-1}(n_\perp/\rho) \\ &\approx n_\perp/\rho\end{aligned} \tag{A.10}$$

and $f_{\mathbf{\Phi}}(\Phi)$ is approximated by the Gaussian distribution $N(\phi, \sigma/\rho)$. This is in contrast to the distribution of magnitude noise, which for $\sigma \ll \rho$ is approximately $N(\phi, \sigma)$. Thus, the standard deviation of phase noise is less than that of magnitude noise by a factor of the signal amplitude.

### *A.4. Derivation of the PDF of the flip angle estimate for the phase-sensitive method*

The signal for a given voxel measured in the first acquisitions in the phase-sensitive technique is denoted as $\rho_1 \mathrm{e}^{\mathrm{i}\phi_1} + \mathbf{n}_1$ and that from the second acquisition is denoted as $\rho_2 \mathrm{e}^{\mathrm{i}\phi_2} + \mathbf{n}_2$, where $\mathbf{n}_1$ and $\mathbf{n}_2$ are two different noise samples. The measured phases from these two acquisitions are denoted as random variables $\mathbf{\Phi}_1$ and $\mathbf{\Phi}_2$ with

$$\mathbf{\Phi}_{1,2} = \arg(\rho_{1,2}\mathrm{e}^{\mathrm{i}\phi_{1,2}} + \mathbf{n}_{1,2}). \tag{A.11}$$

The random variable $\mathbf{\Theta}$ is formed as the difference between the phases of the two excitations,

$$\mathbf{\Theta} = \mathbf{\Phi}_1 - \mathbf{\Phi}_2. \tag{A.12}$$

$\mathbf{\Phi}_1$ and $\mathbf{\Phi}_2$ have PDFs given by equation (A.8) (appendix A.2). The PDF of $\mathbf{\Theta}$ is given by the convolution of the PDFs of $\mathbf{\Phi}_1$ and $\mathbf{\Phi}_2$ (Papoulis 1984):

$$f_{\mathbf{\Theta}}(\Theta) = f_{\mathbf{\Phi}_1}(\Theta) * f_{\mathbf{\Phi}_2}(\Theta), \tag{A.13}$$

which can be evaluated numerically. For the case of $\sigma \ll \rho$, both $\mathbf{\Phi}_1$ and $\mathbf{\Phi}_2$ have nearly Gaussian distributions and the PDF of $\mathbf{\Theta}$ is approximately $N\big(\phi_1 - \phi_2, \frac{\sigma}{\sqrt{1/\rho_1^2 + 1/\rho_2^2}}\big)$.

Calculation of the PDF of $\mathbf{\Theta}$ requires calculation of the nominal (noise-free) magnitude $\rho$ and phase angle $\phi$ of each of the two acquisitions for a given true flip angle $\alpha$. From (Morrell 2008) we have the following expression for the transverse magnetization measured in the two acquisitions:

$$\begin{aligned}M_x &= \pm\frac{M_z^- 4\alpha\Delta\omega\tau}{\beta^2}\sin^2\beta\cos\beta - \frac{M_z^-\alpha\sin\beta}{\beta^3}(\alpha^2\cos 2\beta + \Delta\omega^2\tau^2) \\ M_y &= \pm\frac{M_z^- 2\alpha\sin\beta}{\beta^3}(\Delta\omega^2\tau^2\cos 2\beta + \alpha^2\cos\beta) \\ &\quad + \frac{M_z^-\alpha\Delta\omega\tau}{\beta^4}(1-\cos\beta)(\alpha^2\cos 2\beta + \Delta\omega^2\tau^2),\end{aligned} \tag{A.14}$$

where $\Delta\omega$ is the resonance frequency offset due to the chemical shift or $B_0$ inhomogeneity, $\tau$ is a measure of the RF pulse length and $\beta = \sqrt{\alpha^2 + \Delta\omega^2\tau^2}$. $M_z^-$ represents the longitudinal magnetization available at the beginning of the excitation. The $\pm$ in equation (A.14) is + for the first acquisition with the positive $2\alpha$ initial tip, and $-$ for the second acquisition with the negative $2\alpha$ initial tip. The magnitude of the resulting image is given by

$$\rho = \sqrt{M_x^2 + M_y^2} \tag{A.15}$$

and the phase is given by

$$\phi = \tan^{-1}(M_y/M_x). \tag{A.16}$$

We define a random variable $\mathbf{a}$ as the flip angle estimate. Once the PDF of $\boldsymbol{\Theta}$ has been calculated for given values of the flip angle $\alpha$, off-resonance phase accrual $\Delta\omega\tau$ (depending on off-resonance frequency $\Delta\omega$ and RF pulse length $\tau$), sequence timing parameters TR and $TR_{min}$, and the $T_1$ of the sample, the PDF of $\mathbf{a}$ can be calculated using the function

$$\mathbf{a} = g(\boldsymbol{\Theta}), \tag{A.17}$$

which relates the measured phase angle difference $\boldsymbol{\Theta}$ to the flip angle $\mathbf{a}$. Specifically, the PDF of $\mathbf{a}$ is given by (A.17)

$$f_{\mathbf{a}}(a) = \frac{f_{\Theta}(g^{-1}(a))}{|g'(g^{-1}(a))|} \tag{A.18}$$

where $g^{-1}$ is the inverse of $g$ and $g'$ is the derivative of $g$ with respect to its argument.

For the phase-sensitive $B_1$ mapping technique, the closed form of $g$, $g^{-1}$ and $g'$ is not straightforward, so we have evaluated them numerically.

### *A.5. Derivation of the PDF of the flip angle estimate for the dual-angle GRE method*

We define the random variable $\mathbf{m}_1 = |\rho_1 e^{i\phi_1} + \mathbf{n}_1|$ as the magnitude of the first acquisition, and $\mathbf{m}_2 = |\rho_2 e^{i\phi_2} + \mathbf{n}_2|$ as the magnitude of the second acquisition. Both $\mathbf{m}_1$ and $\mathbf{m}_2$ have the Rician distribution given in equation (A.6) (appendix A.2). Forming the ratio of the two acquisitions gives the random variable

$$\mathbf{r} = \mathbf{m}_1/\mathbf{m}_2. \tag{A.19}$$

Since the noise in the two acquisitions is independent, the two magnitudes have a joint PDF equal to the product of their individual PDFs, i.e.

$$f_{\mathbf{m}_1,\mathbf{m}_2}(m_1, m_2) = f_{\mathbf{m}_1}(m_1) f_{\mathbf{m}_2}(m_2). \tag{A.20}$$

The PDF of $\mathbf{r}$ is calculated from this joint density according to (Papoulis 1984)

$$f_{\mathbf{r}}(r) = \int_{-\infty}^{\infty} |\xi| f_{\mathbf{m}_1,\mathbf{m}_2}(r\xi, \xi)\, d\xi. \tag{A.21}$$

If $\rho_1 \gg \sigma$ and $\rho_2 \gg \sigma$, then both $f_{\mathbf{m}_1}(m)$and $f_{\mathbf{m}_2}(m)$ are nearly Gaussian with means $\rho_1$ and $\rho_2$, respectively, and the PDF of $\mathbf{r}$ can be approximated by (Papoulis 1984)

$$f_{\mathbf{r}}(r) = \frac{1}{\pi(r^2+1)} \exp\left(-\frac{\rho_1^2+\rho_2^2}{2\sigma^2}\right) + \frac{r\rho_1+\rho_2}{\sqrt{2\pi}\sigma(r^2+1)^{3/2}} \times \exp\left(-\frac{(r\rho_2-\rho_1)^2}{2\sigma^2(r^2+1)}\right) \operatorname{erf}\left(\frac{r\rho_1+\rho_2}{\sigma\sqrt{2(r^2+1)}}\right) \tag{A.22}$$

with the error function defined as

$$\operatorname{erf}(u) = \frac{2}{\sqrt{\pi}} \int_0^u e^{-y^2} dy. \tag{A.23}$$

However, the assumption that $\rho_1 \gg \sigma$ and $\rho_2 \gg \sigma$ does not hold for $\alpha$ near $0^\circ$ or as $\alpha$ approaches $90^\circ$ and the PDF of $\mathbf{r}$ must be calculated by numerical integration of equation (A.21).

The noise-free signal magnitudes $\rho_1$ and $\rho_2$ of the two acquisitions can be calculated as

$$\rho_1 = M_z^- \sin\alpha \tag{A.24}$$

and

$$\rho_2 = M_z^- \sin 2\alpha \tag{A.25}$$

where $M_z^-$ is given by equation (3).

Having calculated the PDF of $\mathbf{r}$, we calculate the PDF of the flip angle estimate $\mathbf{a}$ according to

$$f_{\mathbf{a}}(a) = \frac{f_{\mathbf{r}}(g^{-1}(a))}{|g'(g^{-1}(a))|}, \tag{A.26}$$

where the function $g$ relates the measured ratio $\mathbf{r}$ to the flip angle estimate $\mathbf{a}$:

$$\mathbf{a} = g(\mathbf{r}). \tag{A.27}$$

For the dual-angle GRE method,

$$\begin{aligned} g(r) &= \cos^{-1}\left(\frac{1}{2r}\right), \\ g^{-1}(a) &= \frac{1}{2\cos a}, \\ g'(r) &= \frac{1}{r\sqrt{4r^2-1}}. \end{aligned} \tag{A.28}$$

*A.6. Derivation of the PDF of flip angle estimate for the extended dual-angle method*

For this analysis, we have designated the two acquisitions in the extended dual-angle method as 'in phase' if the phase of the second acquisition differs from the phase of the first acquisitions by less than $\pm 90^\circ$. These measurements are interpreted as representing flip angles between $0^\circ$ and $90^\circ$. The two acquisitions are considered to be 'out of phase' if the phase of the second acquisition varies from that of the first acquisition by more than $\pm 90^\circ$. These measurements are interpreted to represent flip angles from $90^\circ$ to $180^\circ$. As for the non-extended dual-angle method, the noise-corrupted image magnitude of the two acquisitions is represented by the random variables $\mathbf{m}_1 = |\rho_1 e^{i\phi_1} + \mathbf{n}_1|$ and $\mathbf{m}_2 = |\rho_2 e^{i\phi_2} + \mathbf{n}_2|$. The noise-corrupted image phase is represented by the random variables $\mathbf{\Phi}_1 = \arg(\rho_1 e^{i\phi_1} + \mathbf{n}_1)$ and $\mathbf{\Phi}_2 = \arg(\rho_2 e^{i\phi_2} + \mathbf{n}_2)$. The noise-free image magnitudes $\rho_1$ and $\rho_2$ are given by equations (A.24) and (A.25), respectively, the same as for the non-extended dual-angle method.

To calculate the PDF of the flip angle estimate for this extended dual-angle GRE method, we need the PDF of the ratio of the two acquisition magnitudes $\mathbf{m_1}$ and $\mathbf{m_2}$, which can be calculated from the joint PDF of $\mathbf{m_1}$ and $\mathbf{m_2}$ as shown in equation (A.21). To incorporate the phase of the two acquisitions into this analysis, we will designate the ratio $\mathbf{r} = \mathbf{m_1}/\mathbf{m_2}$ as positive if the two acquisitions are in-phase and negative if they are out of phase.

Because the noise in the two acquisitions is independent, the joint PDF of the magnitude and phase of both acquisitions is given by

$$f_{\mathbf{m_1},\mathbf{m_2},\mathbf{\Phi_1},\mathbf{\Phi_2}}(m_1, m_2, \Phi_1, \Phi_2) = f_{\mathbf{m_1},\mathbf{\Phi_1}}(m_1, \Phi_1) f_{\mathbf{m_2},\mathbf{\Phi_2}}(m_2, \Phi_2) \tag{A.29}$$

with the joint PDF of the magnitude and phase of each acquisition $f_{\mathbf{m}_{1,2}\,\mathbf{\Phi}_{1,2}}(m_{1,2}, \Phi_{1,2})$ given by equation (A.5) (appendix A.2). Then for positive $\mathbf{r}$, corresponding to in-phase signal acquisitions, the joint PDF of $\mathbf{m_1}$ and $\mathbf{m_2}$ is

$$f^+_{\mathbf{m_1},\mathbf{m_2}}(m_1, m_2) = \int_0^{2\pi} \int_{\Phi_2-\pi/2}^{\Phi_2+\pi/2} f_{\mathbf{m_1},\mathbf{m_2},\mathbf{\Phi_1},\mathbf{\Phi_2}}(m_1, m_2, \Phi_1, \Phi_2)\, d\Phi_1\, d\Phi_2, \tag{A.30}$$

while for negative $\mathbf{r}$, corresponding to out-of-phase signal acquisitions, the joint PDF of $\mathbf{m_1}$ and $\mathbf{m_2}$ is

$$f^-_{\mathbf{m_1},\mathbf{m_2}}(m_1, m_2) = \int_0^{2\pi} \int_{\Phi_2+\pi/2}^{\Phi_2+3\pi/2} f_{\mathbf{m_1},\mathbf{m_2},\mathbf{\Phi_1},\mathbf{\Phi_2}}(m_1, m_2, \Phi_1, \Phi_2)\, d\Phi_1\, d\Phi_2. \tag{A.31}$$

The PDF of the signal ratio **r** is then calculated as

$$f_{\mathbf{r}}(r) = \begin{cases} \displaystyle\int_{-\infty}^{\infty} |\xi| f^{+}_{\mathbf{m}_1,\mathbf{m}_2}(r\xi,\xi)\,\mathrm{d}\xi & \text{for positive } r \\ \displaystyle\int_{-\infty}^{\infty} |\xi| f^{-}_{\mathbf{m}_1,\mathbf{m}_2}(|r|\xi,\xi)\,\mathrm{d}\xi & \text{for negative } r. \end{cases} \tag{A.32}$$

The relationships between the measured magnitude ratio **r** and flip angle estimate **a** are given by

$$\begin{aligned} g(r) &= \cos^{-1}\left(\frac{1}{2r}\right) \\ g^{-1}(a) &= \frac{1}{2\cos a} \\ g'(r) &= \frac{1}{|r|\sqrt{4r^2-1}}, \end{aligned} \tag{A.33}$$

which are nearly the same as for the limited dual-angle GRE method.

### *A.7. Derivation of the PDF of the flip angle estimate for the AFI method*

We will denote the magnitude of the noise-free image formed with the shorter $\mathrm{TR}_1$ as $\rho_1$ and the image formed with the longer $\mathrm{TR}_2$ as $\rho_2$. (This notation is reversed from Yarnykh (2007) for consistency with the above discussion of the other methods.) We again form the random variables $\mathbf{m}_1 = |\rho_1 \mathrm{e}^{\mathrm{i}\phi_1} + \mathbf{n}_1|$, $\mathbf{m}_2 = |\rho_2 \mathrm{e}^{\mathrm{i}\phi_2} + \mathbf{n}_2|$ and $\mathbf{r} = \mathbf{m}_1/\mathbf{m}_2$. Again, the PDFs of $\mathbf{m}_1$ and $\mathbf{m}_2$ are Rician, given by equation (A.6) (appendix A.2), and the PDF of **r** is given by equations (A.21) and (A.22).

Expressions for $\rho_1$ and $\rho_2$ are obtained from Yarnykh (2007), neglecting $\mathrm{T}_2$ relaxation, as

$$\rho_1 = M_0 \sin\alpha \frac{1 - E_1 + (1 - E_2)\,E_1 \cos\alpha}{1 - E_1 E_2 \cos^2\alpha} \tag{A.34}$$

and

$$\rho_2 = M_0 \sin\alpha \frac{1 - E_2 + (1 - E_1)\,E_2 \cos\alpha}{1 - E_1 E_2 \cos^2\alpha} \tag{A.35}$$

with $E_1 = \exp(-\mathrm{TR}_1/T_1)$ and $E_2 = \exp(-\mathrm{TR}_2/T_1)$. Having the PDF of **r**, we calculate the PDF of the flip angle estimate **a** according to equation (A.26) with

$$\begin{aligned} g(r) &= \cos^{-1}\left(\frac{rn - 1}{n - r}\right) \\ g^{-1}(a) &= \frac{1 + n\cos a}{n + \cos a} \\ g'(r) &= \frac{-\sqrt{n^2 - 1}}{(n - r)\sqrt{1 - r^2}}. \end{aligned} \tag{A.36}$$

### *A.8. Derivation of the PDF of the flip angle estimate for the extended AFI method*

As for the AFI method, we form the random variables $\mathbf{m}_1 = |\rho_1 \mathrm{e}^{\mathrm{i}\phi_1} + \mathbf{n}_1|$ and $\mathbf{m}_2 = |\rho_2 \mathrm{e}^{\mathrm{i}\phi_2} + \mathbf{n}_2|$ representing the magnitude of the two acquisitions. We define the random variables $\mathbf{\Phi}_1 = \arg(\rho_1 \mathrm{e}^{\mathrm{i}\phi_1} + \mathbf{n}_1)$ and $\mathbf{\Phi}_2 = \arg(\rho_2 \mathrm{e}^{\mathrm{i}\phi_2} + \mathbf{n}_2)$ as the phase of the two acquisitions. We define the ratio $\mathbf{r} = \mathbf{m}_1/\mathbf{m}_2$ as positive if the phase of the two acquisitions differs by less than $\pm 90^\circ$, and negative if the phase of the second acquisition differs from the

phase of the first acquisition by more than $\pm 90^\circ$. The noise-free image magnitudes $\rho_1$ and $\rho_2$ are given by equations (A.34) and (A.35). The PDF of $\mathbf{r}$ is then found using the same method outlined for the extended dual-angle method, expressed in equations (A.29)–(A.32). From the PDF of $\mathbf{r}$, the flip angle estimate is formed according to equation (A.26) with the function $g(\mathbf{r})$ having the same form as for the non-extended AFI method, given by equation (A.36).

## References


Axel L, Costantini J and Listerud J 1987 Intensity correction in surface-coil MR imaging *Am. J. Roentgenol.* **148** 418–20

Blachman N 1981 The effect of phase error on DPSK error probability *IEEE Trans. Commun.* **29** 364–5

Cunningham C H, Pauly J M and Nayak K S 2006 Saturated double-angle method for rapid B1+ mapping *Magn. Reson. Med.* **55** 1326–33

Deoni S C, Rutt B K and Peters T M 2003 Rapid combined T1 and T2 mapping using gradient recalled acquisition in the steady state *Magn. Reson. Med.* **49** 515–26

Haykin S 2001 *Communication Systems* (New York: Wiley)

Henkelman R M 1985 Measurement of signal intensities in the presence of noise in MR images *Med. Phys.* **12** 232–3

Insko E and Bolinger L 1993 Mapping of the radiofrequency field *J. Magn. Reson.* **103** 82–5

Katscher U, Bornert P, Leussler C and Van Den Brink J S 2003 Transmit SENSE *Magn. Reson. Med.* **49** 144–50

Kerr A B, Cunningham C H, Pauly J M, Piel J E, Giaquinto R O, Watkins R D and Zhu Y 2007 Accelerated B1 mapping for parallel excitation *Proc. 15th Annual Meeting of ISMRM (Berlin, 2007)* p 352

McVeigh E, Bronskill M and Henkelman R 1986 Phase and sensitivity of receiver coils in magnetic resonance imaging *Med. Phys.* **13** 806–14

Morrell G R 2008 A phase-sensitive method of flip angle mapping *Magn. Reson. Med.* **60** 889–94

Morrell G and Schabel M C 2009 A noise analysis of flip angle mapping methods *17th Meeting ISMRM (Hawaii, 2009)* p 376

Moyher S E, Vigneron D B and Nelson S J 1995 Surface coil MRI of the human brain with analytic reception profile correction *J. Magn. Reson. Imaging* **5** 139–44

Nehrke K 2009 On the steady-state properties of actual flip angle imaging (AFI) *Magn. Reson. Med.* **61** 84–92

Papoulis A 1984 *Probability, Random Variables, and Stochastic Processes* (New York: McGraw-Hill)

Roemer P B, Edelstein W A, Hayes C E, Souza S P and Mueller O M 1990 The NMR phased array *Magn. Reson. Med.* **16** 192–225

Schabel M C and Morrell G R 2009 Uncertainty in T(1) mapping using the variable flip angle method with two flip angles *Phys. Med. Biol.* **54** N1–8

Schabel M C and Parker D L 2008 Uncertainty and bias in contrast concentration measurements using spoiled gradient echo pulse sequences *Phys. Med. Biol.* **53** 2345–73

Stollberger R and Wach P 1996 Imaging of the active B1 field *in vivo Magn. Reson. Med.* **35** 246–51

Wade T and Rutt B 2007 Comparison of current B1 mapping techniques *15th Meeting ISMRM (Berlin, 2007)* p 354

Yarnykh V L 2007 Actual flip-angle imaging in the pulsed steady state: a method for rapid three-dimensional mapping of the transmitted radiofrequency field *Magn. Reson. Med.* **57** 192–200

Zhu Y 2004 Parallel excitation with an array of transmit coils *Magn. Reson. Med.* **51** 775–84